Design and Reconstruction of the Viking Lander Descent Trajectories

E.A. Euler,* G.L. Adams,† and F.W. Hopper‡
Martin Marietta Corporation, Denver, Colo.

The design of the Viking descent trajectory, sequence of events, and associated onboard guidance parameters evolved over many years and changed frequently as the design of the Viking Lander matured. An extremely conservative approach was taken in the design of all descent mission phases due to the lack of previous experience with a spacecraft of this type, the desire to provide maximum margin since the entire descent was accomplished without ground intervention, and the large degree of uncertainty in the Mars environment (atmosphere density profile, winds, terrain characteristics) that existed prior to the mission. This paper discusses the final Viking Lander preflight capability, the rationale for the trajectory design, and the postflight reconstruction. The latter includes the reconstructed flight path, landing site errors, and engineering estimates of the Mars environment.

Introduction

THE two Viking spacecraft, consisting of the Viking Orbiter (VO), Viking Lander (VL), and the VL adapter were launched from Cape Kennedy aboard Titan III E/Centaurs on Aug. 20 and Sept. 9, 1975, respectively. After a series of midcourse correction maneuvers, the two spacecraft were injected into Mars orbit on June 19 and Aug. 7, 1976. After the difficult task of finding an acceptable landing site, Viking Lander 1 landed on the surface of Mars on July 20 at 11:53:06 UTC. Viking Lander 2 landed on Sept. 3 at 22:37:50 UTC. All four vehicles are still operating successfully today and have sent back a wealth of scientific information about Mars. References 1-8 are representative papers dealing with various aspects of the entire mission.

The final spacecraft orbit from which the VL descents were made was highly elliptic ($e=0.76$) with a Mars-synchronous period of 24.62 h and a periapsis altitude of 1500 km above the Mars surface. The orbit orientation was selected to achieve the desired target latitude and sun elevation angle when the VO was over the landing site. The VL was separated from the VO at a true anomaly of 217 deg (Fig. 1), and after coasting several minutes to achieve the necessary separation between vehicles, an attitude maneuver was made to achieve the desired inertial orientation for the deorbit burn.

After completion of the 22-min burn, the vehicle maintained the desired inertial attitude until shortly before entry into the Mars atmosphere. During this inactive period of about 3 h, the attitude control system (ACS) engine pulses were monitored and commanded to achieve at least four pulses ever 70 s to prevent engine freeze. Accurate modeling of this mission phase was necessary to maintain the desired trajectory accuracy.

The atmospheric entry point was defined to be at 243.8 km (800,000 ft) above the Mars reference surface (areoid), although significant aerodynamic forces did not occur until much lower. The areoid is the equipotential surface derived from Mariner 9 data and defined in Ref. 9. At 9 min prior to entry another attitude maneuver was performed to properly orient the vehicle body axes with respect to the relative velocity vector (angle of attack $= -20$ deg) to acquire upper atmosphere science data. Also, a programmed pitch rate was initiated to follow the flight path angle change and maintain the desired angle of attack.

At entry a step change was made in pitch to achieve the desired angle of attack of -11.1 deg. The vehicle attitude was actively controlled until 0.05 g was sensed at an altitude of about 91 km. At this time the vehicle was allowed to trim to the aerodynamic equilibrium angles of attack and sideslip. Pitch and yaw rates were controlled to be less than 1 deg/s and roll control was achieved by keeping the yaw axis perpendicular to the local vertical direction.

At a sensed condition of 5.79 km above the local terrain, the parachute was deployed and 7 s later the aeroshell was jettisoned. At this time the terminal descent propulsion system roll thrusters were activated to provide roll control and the vehicle remained uncontrolled in pitch and yaw until terminal descent engine ignition.

At a sensed altitude of 1.49 km above the terrain the main terminal descent engines (3) were ignited. The engines were warmed up for 2 s, at which time the parachute and basecover were separated. The VL then pitched into the relative velocity and performed a gravity turn to near-touchdown while following a preprogrammed altitude-velocity profile. At a sensed condition of 16.8 m or 2.4 m/s relative velocity the VL descended vertically to the surface at constant speed. When touchdown was sensed, the propulsion system was sealed and the landed mission program begun.

Preflight Capability

The relevant preflight system and mission constraints are summarized next. Because of VL aeroshell structural limitations the maximum dynamic pressure ($q_{max.}$) experienced by the VL during entry could not exceed 144 psf. The total stagnation heat load (Q) during entry could not exceed 1510 btu/ft^2, while the stagnation heating rate ($\dot{Q}$) could not exceed 26 btu/ft^2 – s. At parachute deployment the dynamic pressure (q_D) had to be between 5.0 and 8.6 psf and the Mach number (M_D) less than 2.1. The maximum deorbit ΔV of 156 m/s was determined by propellant loaded, propellant margin, and VL mass. VL thermal and power constraints dictated that VL coast time from deorbit to entry could not exceed 5 h. Finally, in order to insure required bit error rates during data transmission from the VL to the VO during descent and the initial postland link, the relative VL/VO geometry had to provide for relay communications

Presented at the AAS/AIAA Astrodynamics Specialist Conference, Jackson Hole, Wyo., Sept. 7-9, 1977; submitted Nov. 11, 1978; revision received March 10, 1978.

Index categories: Entry Vehicle Mission Studies and Flight Mechanics; Entry Vehicles and Landers; Spacecraft Navigation, Guidance, and Flight-Path Control.

*Chief, Mission Analysis Section. Member AIAA.
†Senior Staff Engineer, Mission Analysis Section. Member AIAA.
‡Formerly Senior Staff Engineer. Member AIAA.

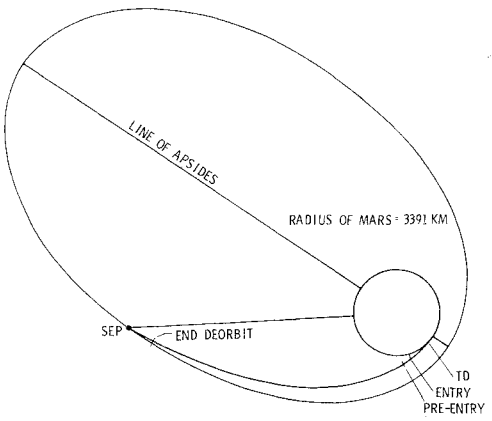

Fig. 1 Nominal VL descent trajectory.

system performance which exceeded the sum of adverse tolerances and permitted an initial link duration of at least 10.4 min. In addition, it was desired to minimize the entry weight (or equivalently, use the maximum ΔV capability, thereby maximizing deorbit propellant usage within constraints) and select trajectories to minimize the landed dispersions.

All of these constraints were satisfied under stacked worst-case conditions. Worst-case conditions were obtained by selecting each relevant statistical error source at its 3σ magnitude and with its worst-case sign. Winds were selected at their 99% magnitude and in the worst-case direction. In addition, the worst-case atmosphere model was selected from one of the five equally probable atmosphere models shown in Fig. 11.

This was not the entire set of constraints to be satisfied. However, they were the constraints which governed the design of the descent trajectory. Other constraints, which were satisfied by orienting the VL attitude properly during descent, will be discussed in a subsequent paragraph.

One of the key concepts for expressing VL capability is that of accessible area. The accessible area is that region in inertial space within which the VL could land from a given separation orbit without violating mission or system constraints. As the VL trajectory design evolved, the accessible area became progressively reduced in size as new system requirements and desires became known. In the following discussion, the three major accessible area concepts will be presented. The first accessible area is termed the maximum accessible area. This accessible area represents the region in which the VL could land if it were utilizing its maximum capabilities and if there were no trajectory dispersions. The second accessible area is termed the targeting region, and reflects entry corridor (γ_E) dispersions and a more conservative utilization of VL capabilities. The third accessible area is termed the preferred targeting region, and refers to a small entry flight path angle band of ± 0.1 deg centered about the nominal entry flight path angle. This region was employed in the targeting of the final VO site acquisition maneuvers and the final design of VL descent trajectories. It reflects a design objective introduced by project management during flight operations in order to maximize the probability of mission success.

Maximum Accessible Area

The procedure for constructing the maximum accessible area will be described and, in so doing, it will be shown how all of the constraints summarized earlier were satisfied. The process begins by determining the entry corridor, i.e., the γ_E region between the steepest and shallowest permissible entry flight path angle at fixed entry altitude. The entry corridor is determined by the entry phase constraints on $q_{\max}$, Q, $\dot{Q}$, q_D, and M_D. These parameters were examined over a broad range of entry flight path angles, for all five equally probable

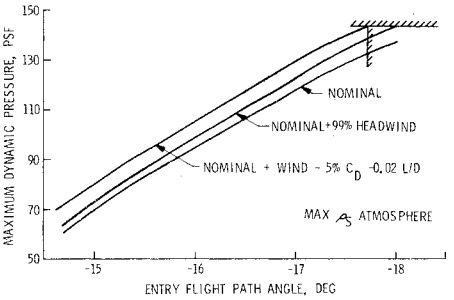

Fig. 2 Sensitivity of $q_{\max}$ to entry errors.

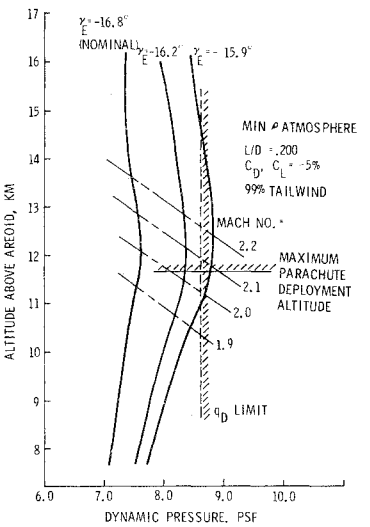

Fig. 3 Parachute phase dynamic pressure and Mach number vs altitude.

Martian atmospheres, and with worst-case winds and VL aeroshell aerodynamic characteristics. Figure 2 shows that the maximum $q_{\max}$ was attained in the max ρ_s atmosphere with a 99% headwind, 5% (3σ) low aeroshell C_D, and a 0.02 (3σ) low L/D. The steepest γ_E permitted under these conditions was $\gamma_E = -17.7$ deg, since $q_{\max}$ equaled the constraint value of 144 psf at this value of γ_E. Although the shallowest conceivable entry flight path angle is the skip-out flight path angle, which was -13.5 deg, the shallowest permissible entry flight path angle was actually determined by the parachute deployment constraints. Figure 3 shows q_D and M_D vs altitude above the areoid (near the end of the aeroshell phase) for a range of entry flight path angles. The worst-case conditions which maximized q_D and M_D are listed on the figure. This figure suggests that γ_E could not be more shallow than -16 deg in order to satisfy the parachute deployment constraints. An earlier analysis showed that the constraints could be satisfied at the same altitude for γ_E of -15.9 deg. Subsequent environmental model adjustments shifted the curves, causing a minor violation of the deployment dynamic pressure for $\gamma_E = -15.9$ deg. The project decided to accept this minor constraint violation rather than change the deployment altitude, which would have caused a redesign of other parameters in terminal descent. A similar sensitivity analysis was performed for Q and $\dot{Q}$ and showed that these constraints were also satisfied between the upper and lower bounds.[10] Thus, the VL entry corridor was bounded by a shallow γ_E of -15.9 deg and a steep γ_E of -17.7 deg.

It will be useful at this point to define relevant descent parameters to aid in the remaining discussion of the maximum accessible area. Cone angle (CA) is the in-plane thrust pointing angle; clock angle (CLA), the out-of-plane thrust pointing angle. Entry lead angle (λ_E) is defined as the angular separation betweeen the VL and the VO when the VL arrives at the entry radius. A negative lead angle means the VL is leading the VO , and this is the normal situation. The PER

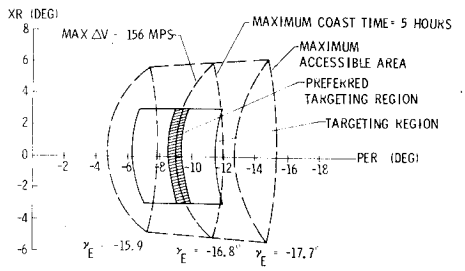

Fig. 4 Targeting regions.

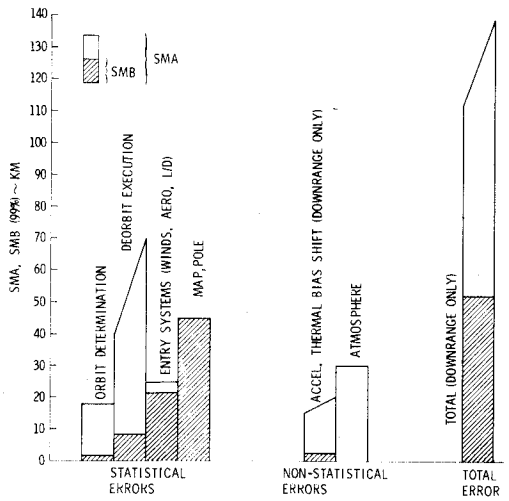

Fig. 5 Components of touchdown dispersion ellipse SMA and SMB over targeting region.

angle is the angle between VO periapsis and the VL at touchdown. The cross-range angle (XR) is the angular displacement of the VL out of the VO orbital plane at touchdown. Coast time (t_c) is measured from the beginning of the deorbit burn maneuver to entry.

The final step in constructing the VL maximum accessible area was to determine the XR capability for the entry corridor defined earlier. XR capability was determined primarily by maximum deorbit ΔV and t_c. The maximum available deorbit propellant of 160.1 lb was determined by subtracting the ACS propellant and all propellant margins from the total propellant loaded in the tanks. This in turn, along with initial VL mass and deorbit propulsion system I_{sp}, determined a maximum available deorbit ΔV of 156 m/s. The maximum coast time was stated earlier to be 5 h, and resulted from a worst-case power and thermal analysis for VL descent. Finally, analysis showed that for the entry corridor specified earlier, a lead angle of -20 deg would always permit satisfaction of the descent and initial postland relay link constraints. These three parameters—ΔV of 156 m/s, t_c of 5 h, and λ_E of -20 deg, and the entry corridor specified earlier, completely defined the maximum accessible area shown in Fig. 4. Each convex subregion in this figure corresponded to a specified entry flight path angle and was determined by the maximum ΔV and t_c boundaries.

Targeting Region and Preferred Targeting Region

The targeting region is a subregion of the maximum accessible area and is obtained by acknowledging entry flight path angle dispersions due to orbit determination and deorbit execution errors, and by utilizing VL capabilities in a more conservative fashion. To protect against entry flight path angle dispersions causing entry outside the entry corridor, it was necessary to constrict the entry corridor on both the shallow and steep boundaries by the expected (3σ) γ_E dispersions. These dispersions increased significantly with XR and, to a lesser extent, with γ_E.[10] A decision was made to limit the maximum γ_E dispersion, thereby bounding the touchdown dispersion ellipse size. This was accomplished by limiting XR to a ± 3 deg range.

Finally, the deorbit ΔV was set at its maximum value of 156 m/s in order to minimize entry weight and coast time. This had the effect of eliminating the convex subregions for each γ_E in the maximum accessible area and reducing it to a single γ_E arc.

The targeting region obtained by constricting the entry corridor by the γ_E dispersions and by fixing deorbit ΔV at its maximum value is shown in Fig. 4. Also shown is the superimposed maximum accessible area, as well as the third accessible area concept mentioned earlier, the preferred targeting region. This latter region was obtained from the targeting region by defining a mini-entry corridor of ± 0.1 deg about the nominal flight path angle, which for VL1 was -16.8 deg and for VL2 was -17.0 deg. After the nominal entry flight path angle was selected for the actual descent, the final VO site acquisition maneuver was designed to keep the selected landing site within this band.

Landing Accuracy

If the landing site is selected to lie within the targeting region described earlier, we are assured of a descent trajectory which satisfies all relevant system and mission constraints. The measure of the VL's capability of landing close to that selected site is given by the touchdown dispersion ellipse. This 99% ellipse is centered at the nominal touchdown site and is defined by the downrange semimajor axis (SMA) and the crossrange semiminor axis (SMB).

Figure 5 shows both the total SMA and SMB of the touchdown dispersion ellipse, as well as the contribution of each important error source to the total. Statistical components were root-sum-squared to obtain the total statistical error. The total error was obtained by adding the total statistical error to the algebraic sum of the nonstatistical errors. The trapezoidal bars represent the variation in each error source from XR = 0 deg to XR = 3 deg. It should be noted that SMA and SMB showed very little variation over the entry corridor, so that the results shown in Fig. 5 were applicable to the entire targeting region.

Deorbit execution errors resulted from errors in deorbit ΔV magnitude (due to accelerometer bias), in-plane pointing, and out-of-plane pointing. The relative importance of each of these three errors was unusual for the Viking deorbit in that ΔV magnitude was the dominant contributor to γ_E errors and SMA, out-of-plane pointing was the dominant contributor to SMB, while in-plane pointing was an insignificant error source as far as γ_E, SMA and SMB were concerned.

Entry systems errors were comprised of winds and errors in predicting VL aerodynamic characteristics. Each of these two sources made roughly equal contributions to SMA, while SMB was due primarily to winds. Since the direction of the wind was assumed to be random, winds made equal contributions of 19 km to both SMA and SMB. The errors in VL aerodynamics which contributed to SMA were VL L/D, C_L, and C_D errors. This should be apparent since these errors induce errors in the lift and drag vector magnitudes and in-plane directions. The only VL aerodynamic errors which contributed to SMB were the VL entry roll angle and lateral c.g. offset errors. These errors act by tilting the VL lift vector out of the entry plane.

Since the touchdown dispersion ellipse was very important in the selection of a suitable landing site, i.e., the ellipse could not include potentially hazardous surface features, the uncertainty in the location of a given point on the Martian surface also had to be factored into the dispersion ellipse. The two error sources which produced errors in locating a point on the Martian surface were the Martian pole error and the map error. These error sources together made equal contributions of 45 km to both SMA and SMB.

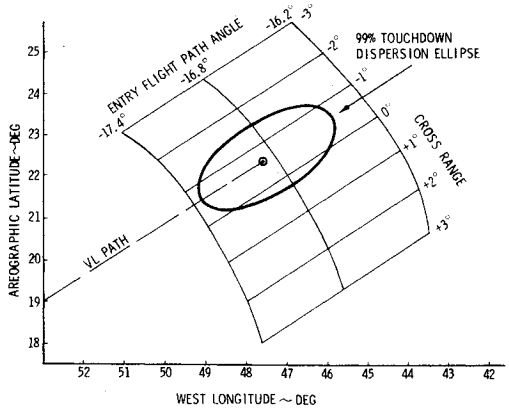

Fig. 6 Final VL1 targeting region and landing site.

The accelerometer thermal bias shift error (ATBS) was a nonstatistical error. The possibility of such an error was postulated during preflight analysis when it was shown that moderately large temperature transients might occur at the accelerometers due to ACS engine firings during deorbit.

Five equally probable atmosphere models were assumed for preflight analyses. Since only one atmosphere can be used for targeting the actual descent trajectory, it is important to know how the touchdown point would be shifted if one of the other atmosphere models were encountered during descent. For Viking, the mean atmosphere model was used for targeting. The maximum displacements of the touchdown point were induced by the min ρ and max ρ models. This should be expected since these were the models having the minimum and maximum upper atmosphere densities, respectively. Since each atmosphere was assumed to be equally probable, the conservative approach was to add this touchdown error algebraically to the total statistical error. The touchdown error due to atmospheres was totally an SMA error, with no contribution whatever to SMB.

Design of the Actual Viking Descent Trajectories

The design of each actual Viking descent trajectory and the corresponding descent guidance parameters began after the final landing site had been selected. For a given separation orbit and epoch, the XR/PER targeting region discussed earlier defined a corresponding latitude/longitude targeting region in which the desired landing site could be selected. If no site within this targeting region was acceptable, the targeting region could be shifted in latitude/longitude space by performing small VO orbital trim maneuvers. For VL1 the targeting region was shifted significantly when VO observations of the primary landing area showed unexpected terrain roughness. For VL2 the targeting region was selected prior to the last scheduled VO orbital trim maneuver.

The final targeting region for VL1 is shown in Fig. 6. Centered about the nominal landing site is the 99% touchdown dispersion ellipse. Also shown in this figure is the predicted ground trace of the VL as it approaches the landing site.

The final targeting region for VL2 was similar, except that the touchdown dispersion ellipse for VL2 was smaller than the preflight ellipse used for VL1. There were several reasons for this. First, analysis of actual VL1 deorbit data showed that temperatures were stable during deorbit and no ATBS had occurred. It was for this reason that the ATBS was deleted as a VL2 error source. Second, the reconstruction process, as expected, was able to reduce the degree of atmospheric uncertainty; consequently, the in-plane nonstatistical touchdown dispersions due to the unknown atmosphere were reduced from ± 30 km for VL1 to ± 12 km for VL2. Third, as a result of landed VL1 tracking, the pole component of the map/pole dispersion was greatly reduced. This permitted the 45×45 km map and pole error contribution used for VL1 to be reduced to 30×30 km for VL2, which essentially was the map error only.

In addition, the nominal VL2 entry flight path angle was selected to be -17.0 deg, unlike the -16.8 deg angle for VL1. There were two reasons for this. First, the fact that VL1 had actually entered with a flight path angle of -17.0 deg and landed successfully provided a strong argument for doing the same thing with VL2. Second, the VL2 site nominal atmosphere extrapolated from the atmosphere reconstructed from the actual VL1 data showed that entry at an angle steeper than -16.8 deg was entirely satisfactory since the characteristics of the reconstructed atmosphere at high altitude meant that a lower $q_{\max.}$ would be encountered.

The targets used to define the final VL trajectories were 1) areographic latitude = 22.6 deg N (VL1), 47.89 deg N (VL2); 2) longitude = 47.5 deg W (VL1), 225.86 deg W (VL2); 3) deorbit $\Delta V = 156$ m/s, and 4) entry lead angle = -20 deg. The selection of deorbit ΔV as a target is consistent with the decision discussed earlier to select the deorbit ΔV at its maximum value in order to minimize coast time and entry weight. Entry lead angle was selected as a target because the targeting region employed in landing site selection was based on a lead angle of -20 deg to insure acceptable descent and initial postland relay link performance. Note that entry flight path angle γ_E was not a target since selection of the landing site within the targeting region automatically determined γ_E (observe the γ_E arcs in Fig. 6).

After the VL descent trajectory had been designed, a corresponding set of descent guidance parameters had to be computed. These constituted a set of commands which were uplinked to the spacecraft and which, when executed, produced the desired descent trajectory. The descent guidance parameters represented the culmination of the descent trajectory design process and guaranteed satisfaction of all trajectory-related constraints and requirements discussed earlier. They also guaranteed satisfaction of certain constraints and requirements imposed on the VL attitude during descent. These attitude-related constraints and requirements are described subsequently as part of the discussion of the specific functions of certain descent guidance parameters.

All VL attitudes prior to entry (E) are defined by the matrix transformation from body axes at separation (SEP) to the desired orientation. This separation coordinate frame was defined by the ideal VO celestial lock orientation corrected for the predicted VO roll drift while the VO was on roll inertial hold from SEP $-$ 3 h to SEP.

The first required orientation after separation was for the deorbit burn. This matrix defined the required pointing of the VL x axis for the deorbit burn, as determined by the targeting process. It also defined the VL roll orientation about the x axis (longitudinal) which resulted in minimum sensitivity of entry flight path angle errors to deorbit pointing errors in the event of excessive tipoff rates at separation (or a VL lateral accelerometer failure).

Following the deorbit burn, the VL was reoriented to prepare for the long coast phase of the descent trajectory. In the case of VL1 a roll maneuver about the x axis was performed to position the VL z axis perpendicular to the sun direction. This maneuver, plus another 180-deg roll midway through the long coast prevented uneven heating of the IRU, which was located on the z axis. In the case of VL2, the reorientation after the deorbit burn involved a repositioning of the x axis as well as a roll about the x axis. The repositioning of the VL2 x axis was required to shield the retarding potential analyzer (RPA) mounted on the aeroshell from the sun during the long coast.

The pre-entry phase for VL1 began at E $-$ 6 min, which required that the attitude maneuver for pre-entry be initiated at E-9 min. The pre-entry phase for VL2 was delayed until E-3 min. in order to keep the sun out of the RPA port while electron temperature measurements were being made. This

required that the VL2 attitude maneuver for pre-entry be initiated at E – 6 min. The VL began a slow pitch maneuver from this attitude in order to maintain the RPA port essentially parallel to the VL relative velocity vector until entry. The slow pitch was interrupted momentarily at entry by a step change in pitch to place the VL in the aerodynamically trimmed orientation. The slow pitch maneuver then maintained this trimmed orientation until aerodynamic moments took over at 0.05 g.

A parachute phase roll command was designed to produce the required VL leg no. 1 azimuth at touchdown, which for VL1 was 320 deg and for VL2 was 210 deg. The VL leg no. 1 azimuth was selected to provide proper relay link performance during postland relay links and optimum camera lighting during real-time imaging sequences when the VO was overhead.

Reconstruction of the Descent Trajectories and Mars Environment

Because of the large degree of uncertainty in the Mars environment discussed earlier and the absence of VL flight test data, plans were made to reconstruct the VL trajectory during mission operations to estimate flight performance and derive engineering estimates of the environment. This was of particular importance after the VL1 descent so that changes could be made in targeting and selection of guidance parameters for VL2, if necessary. In addition, much of the data were necessary to support the entry science investigations of atmosphere structure and composition.

The entry trajectory reconstruction process was used to estimate the position, velocity, and attitude profile from the nominal entry time to touchdown. The entry data used for this reconstruction were provided by 3-axis gyro, accelerometer, radar altimeter (RA), terminal descent and landing (doppler) radar (TDLR), stagnation pressure, recovery temperature, and ambient temperature and pressure measurements. Note that there were no tracking data (e.g., doppler or range) to relate the VL position to the VO or to Earth during entry, except for a landed position fix obtained from direct tracking of the VL after touchdown. The accelerometer and gyro data (called dynamic data) were first edited, smoothed, and filled. Then they were differentiated to produce a continuous time history of angular velocity and acceleration for each vehicle axis.

Using the dynamic data plus the planet gravitational model, the a priori entry state and attitude were propagated forward in time in the manner of a strap-down inertial navigator. In so doing, angular velocity data were integrated to keep track of vehicle attitude, and total acceleration was integrated to provide vehicle velocity and position time histories. At selected time points RA and TDLR measurements were processed with a Kalman-Schmidt filter to correct vehicle state and parameter estimates. After similarly processing the position fix slightly before touchsown, the resulting final state was integrated back to entry to provide a final continuous reconstructed trajectory.

The environmental estimates were then obtained using the final reconstructed trajectory. Working from entry to touchdown, the dynamic pressure was computed from sensed acceleration, using a priori aerodynamic data. Density was computed from dynamic pressure, based on the velocity history from the estimated trajectory (modified by wind estimates). Pressure was computed by integration of density with respect to altitude in the hydrostatic equation. Temperature was then computed from density and pressure by means of the equation of state. Wind estimates were based on a comparison of a priori aerodynamic trim predictions with those computed for the estimated trajectory on a no-wind basis. Pressure and temperature measurements were processed at selected times to provide atmospheric corrections. Finally, a continuous reconstructed atmosphere was obtained by means of a deterministic run of the estimated

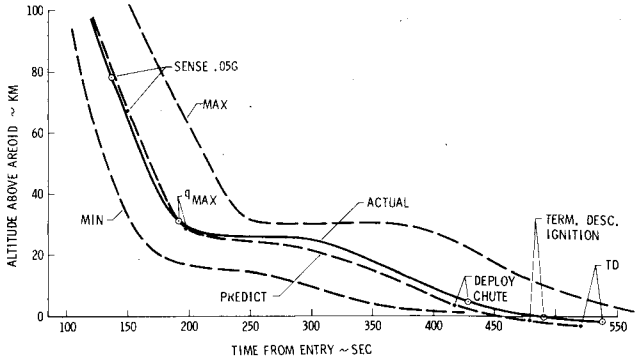

Fig. 7 VL1 predicted vs actual entry trajectory.

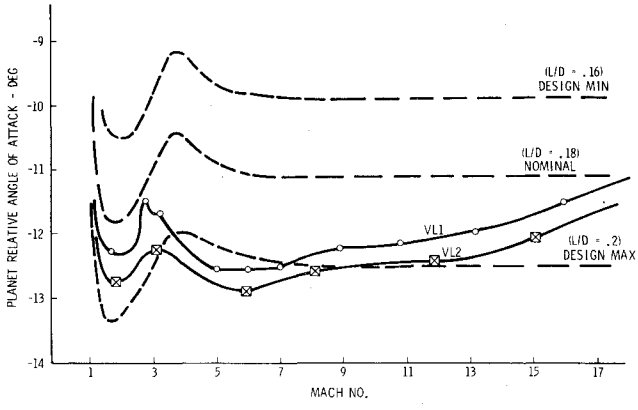

Fig. 8 Reconstructed angle of attack.

trajectory in which were input a wind-vs-altitude table and other parameter estimates from previous filtering runs. A more detailed explanation of this process can be found in Ref. 11.

The actual Viking entry trajectory reconstruction process went very smoothly after a complete set of entry data had been obtained. Much of the preflight analysis of this process was directed toward preparing to cope with large errors and the resulting strong nonlinearities. However, in-flight performance was nearly flawless, with exceptional data quality and subsystem performance. For instance, the fear of a large radar blackout region and a resulting loss of reconstruction accuracy led to studies and development of special procedures, but both landers obtained near-continuous radar altimeter measurements below 130-km altitude.

Figure 7 shows the comparison of the predicted and estimated portions of the lower-altitude part of the trajectory for VL1 along with the preflight predictions of the min. and max. dispersed trajectories. The accuracy of the estimated profile ranges from 0.45 km (1σ) at 0.05 g to 0.2 km at touchdown. The comparison for VL2 is similar and is not shown. Note that the trajectory remained at near-zero flight path angle for a longer time than was predicted due to the combined effect of the actual atmosphere profile encountered and the aerodynamics of the VL.

Figure 8 shows the estimated trim angle of attack (α_{trim}) profile vs Mach number for both landers. The curves for the two landers are qualitatively similar to each other, but differ distinctly in shape from the a priori curves obtained from wind-tunnel testing. Above Mach 3 the reconstructions were based on planet-relative rather than air-relative velocity, but are believed accurate in that unreasonably large winds would be required to alter them significantly. For example, at Mach 5, where flight path angle was approximately zero, the results are virtually insensitive to horizontal wind. There a vertical wind of about 18 m/s would be required to explain a 1-deg difference. Although such a vertical wind may not be totally

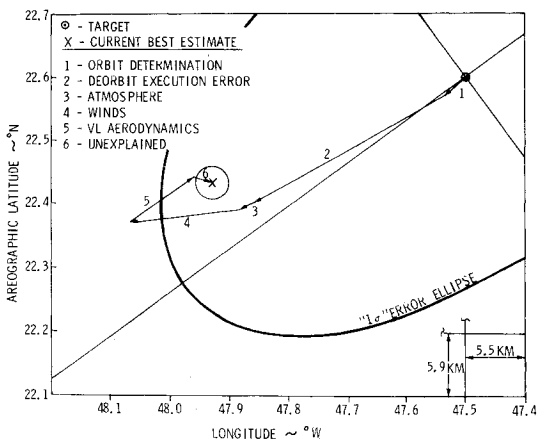

Fig. 9 VL1 landing site error.

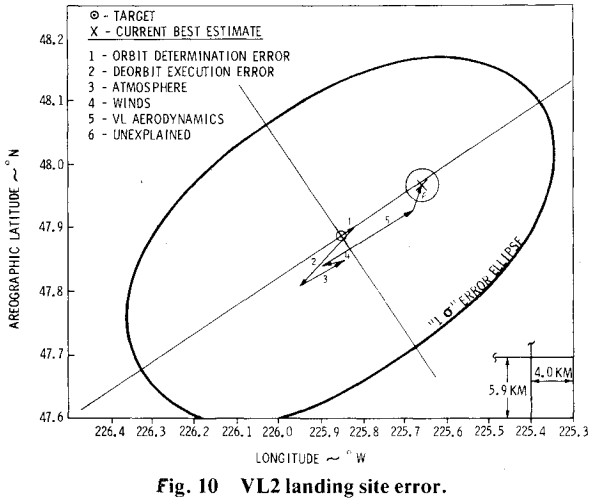

Fig. 10 VL2 landing site error.

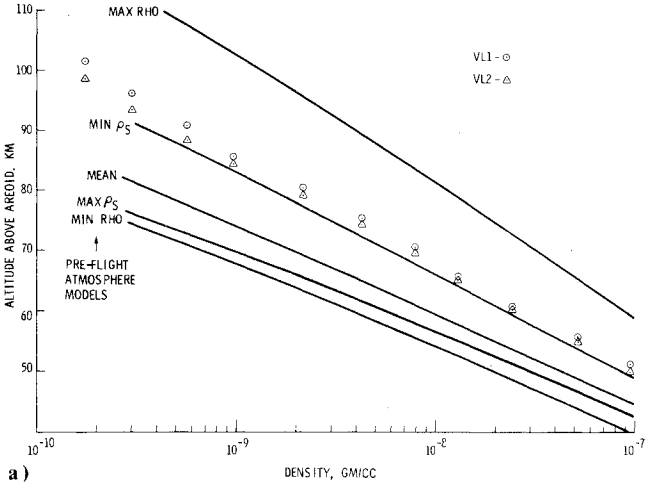

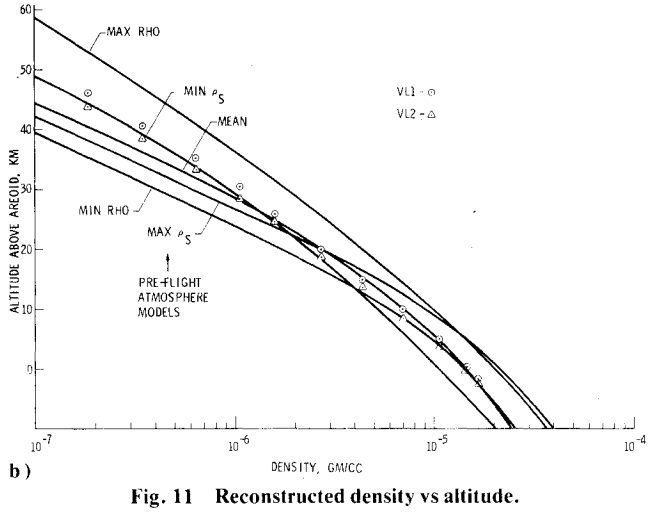

Fig. 11 Reconstructed density vs altitude.

unreasonable considering surface slopes, it was fairly well ruled out as a factor by the similarity of the VL1 and VL2 curves.

Below Mach 3, where winds were being estimated, the accuracy of the a priori curve becomes quite important. Here the estimation process tends to reconstruct a wind which, when combined with planet-relative velocity, results in a reconstructed α_{trim} curve qualitatively similar to the a priori nominal, though biased away from it.

In addition to the foregoing, the axial force coefficients for both VLs were estimated, on the average, to be about 1% higher than the a priori values, and the average value of the parachute drag coefficient was estimated to be about 8% higher than nominal. Both of these estimates were within the preflight uncertainty. Further discussion of the VL aerodynamics can be found in Ref. 12.

Figures 9 and 10 depict the current best estimates of the contributions of all error sources to the VL1 and VL2 landing site errors, respectively. The reconstructed error sources correspond to reconstructed entry state, atmosphere, winds, terrain, and VL L/D characteristics. Note that in the case of VL1, high-altitude winds were not explicitly solved for in the atmospheric reconstruction process. However, there were strong indications of a 30-m/s wind from the East. For VL1 the dominant contributor to the landing site error was the deorbit execution error—more specifically, the deorbit ΔV magnitude error. The errors due to VL aerodynamics and winds were also important. Although the deorbit execution error was also important for VL2, the dominant contributor to the VL2 landing site error was the VL L/D modeling error discussed earlier. The smaller contribution of the deorbit execution error to VL2 is very likely because the VL2 axial accelerometer was more stable than the VL1 axial accelerometer. During VL2 preseparation checkout the accelerometer bias stability data showed very little variability, unlike the relatively large variations which were observed during the VL1 preseparation checkout. In Figs. 9 and 10 are shown two 1σ dispersion ellipses. The large ellipse represents the a priori control dispersions which were predicted prior to separation. The small ellipse represents the knowledge dispersions for the final estimate of the landing site from VL post-touchdown tracking.

The estimate of the density profile obtained from the entry trajectory reconstruction process is shown in Figs. 11a and 11b along with the preflight model profiles. The wind magnitude estimates along with their uncertainty are shown in Fig. 12.

The atmosphere estimation scheme is different during the different flight regimes. At altitudes above 25 km the estimates are quite stable and not dependent on wind estimates. During the phase of near-zero flight path angle, in-plane winds cannot be estimated, yet they can introduce errors in the density computations which can be significant at lower relative velocities. Below 25 km, when the relative flight path angle is less than -6 deg, the winds are estimated using the a priori trim characteristics of the VL with corrections from the stagnation pressure data. Note that the wind uncertainties in Fig. 12 are of the same order of magnitude as the estimates themselves, especially in the case of VL2, for which the winds appear to have been small enough during the aeroshell phase to be ignored in the atmosphere computations.

The wind and atmosphere reconstruction was extremely difficult during the parachute deployment phase due to large

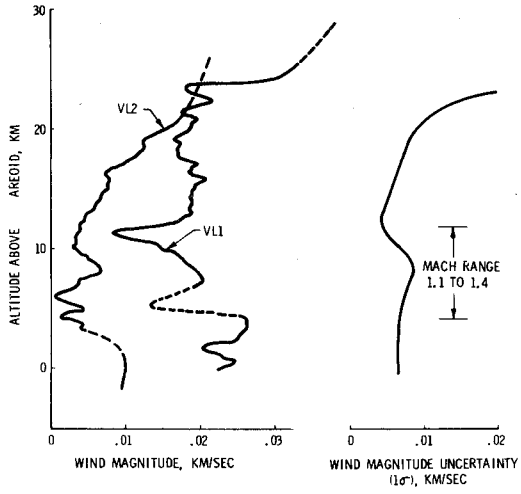

Fig. 12 Reconstructed wind magnitude and uncertainty.

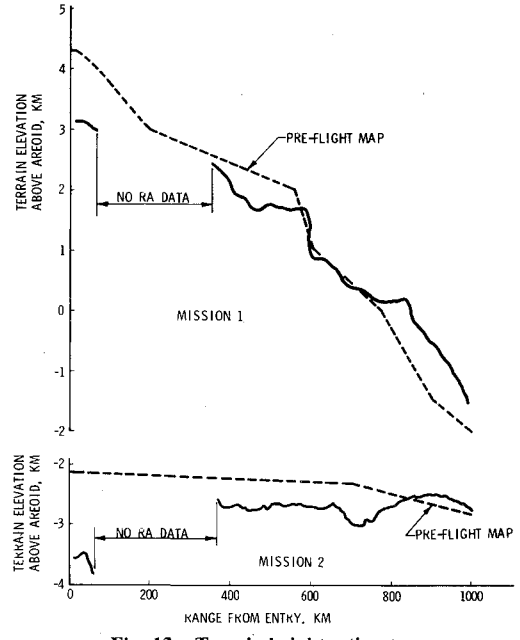

Fig. 13 Terrain height estimates.

amplitude attitude excursions and complicated dynamical motion. After steady state was achieved, the wind estimation algorithm assumed that, on the average, the VL longitudinal axis lay on a 6-deg cone about the air-relative velocity vector. A horizontal wind was then defined by the difference between planet-relative and air-relative velocity vectors. Inherent in this approach was an error during most of the parachute phase (after the initial rapid decrease in relative velocity to around 60 m/s) of about 6 m/s in the horizontal wind estimate. Final results incorporated parachute drag coefficient scale factor estimates based on ambient pressure and temperature measurements processed during the parachute phase and post-touchdown.

The engineering estimates of the atmosphere reported herein were products of the near-real-time activity during Viking mission operations and do not incorporate all of the available science instrument data. More complete and detailed results can be found elsewhere (see, for instance, Ref. 13).

Overall, the atmosphere characteristics were quite favorable from a vehicle design point of view. A high-density scale height in the upper atmosphere resulted in a more gradual deceleration of the VL, thereby lowering the maximum dynamic pressure and the conditions at parachute deployment. This was a factor in targeting VL2 slightly steeper than VL1. In the lower atmosphere, the density was near the expected value and, when coupled with the moderate winds experienced, resulted in nominal performance during the parachute and terminal descent phase, well away from design boundaries. The propellant consumption for both vehicles during terminal descent was within a few pounds of the nominal value, with a resultant propellant margin of almost 30 lb (12%).

One final environmental parameter, terrain height during approach to the landing site, was derived from the reconstruction process. The terrain profiles in Fig. 13 were obtained by comparing altitude estimates of the VL1 and VL2 reconstructed trajectories with corresponding radar altimeter measurements. Also shown on the figure are the profiles deduced from preflight Mars topographical maps. The a priori uncertainty in the terrain height was 1 km (1σ). As can be seen from the figure, the estimates compare favorably with the preflight maps. The 1σ uncertainty associated with the VL1 terrain height estimates varies from about 0.2 km at touchdown to 0.9 km at entry. For the VL2 estimates corresponding uncertainties are 0.5 and 1.0.

Acknowledgment

The work reported in this paper was conducted under Contract NAS1-9000 under the management of NASA Langley Research Center. The authors would like to acknowledge their colleagues on the Viking Flight Team, all of whom made significant contributions to this effort: C.E. French, D.L. Mann, T.P. Garrison, and J.P. McGuire of Martin Marietta Corporation; J.W. Gerschultz of G.E., and J.T. Findlay of AMA. The authors would also like to thank W.J. O'Neil of JPL, whose leadership of the Flight Path Analysis Group contributed much to the overall success of the Viking mission.

References

[1] Goodlette, J.D., "From Separation to Touchdown: The Performance of the Lander Capsules," AIAA Paper 77-269, Jan. 1977.

[2] Martin, J.S., "A Viking Overview," AIAA Paper 77-267, Jan. 1977.

[3] Lee, B.G., "Design and Implementation of the Viking Mission," AIAA Paper 77-270, Jan. 1977.

[4] Lyman, P.T., "Viking Orbiter Spacecraft: A Comparison of Design Requirments and Operational Performance," AIAA Paper 77-268, Jan. 1977.

[5] Euler, E.A., "Navigating the Viking Lander," *The Institute of Navigation National Aerospace Meeting,* Denver, Colo., April 1977.

[6] O'Neil, W.J., "An Overview of Viking Navigation," *The Institute of Navigation National Aerospace Meeting,* Denver, Colo., April 1977.

[7] Hildebrand, C.E., et al., "Viking Satellite Orbit Determination," AIAA Paper 77-70, Calif., Jan. 1977; published also *Journal of Guidance and Control,* to be published.

[8] Ingoldby, R.N., "Guidance and Control System Design of the Viking Planetary Lander," AIAA Paper 77-1060, Hollywood, Fla., Aug. 1977; also, *Journal of Guidance and Control* Vol. 1, May-June 1978, pp. 189-196.

[9] Christensen, E.J., "Martian Topography Derived from Occultation, Radar, Spectral, and Optical Measurements," *Journal of Geophysical Research,* Vol. 80, July 1975.

[10] Euler, E.A., Adams, G.L., and Hopper, F.W., "The Design and Reconstruction of the Viking Lander Descent Trajectories," *AAS/AIAA Astrodynamics Specialist Conference,* Jackson Hole, Wyo., Sept. 1977.

[11] Hopper, F.W., "Trajectory, Atmosphere, and Wind Reconstruction from Viking Measurements," AAS Paper No. 75-068, *AAS/AIAA Astrodynamics Conference,* Nassau, Bahamas, July 1975.

[12] Kirk, D.B., Intrieri, P.F., and Seiff, A., "Aerodynamic Behavior of the Viking Entry Vehicle: Ground Test and Flight Results," AIAA Paper 77-1160, Hollywood, Fla., Aug. 1977; also *Journal of Spacecraft and Rockets*, Vol. 15, July-Aug. 1978.

[13] Seiff, A. and Kirk, D.B., "The Structure of the Atmosphere of Mars in Summer at Mid-Latitudes," *Journal of Geophysical Research,* to be published.